The *Escherichia coli* large ribosomal subunit at 7.5 Å resolution

Rishi Matadeen[1], Ardan Patwardhan[1], Brent Gowen[1], Elena V Orlova[1], Tillmann Pape[1], Marianne Cuff[1], Florian Mueller[2], Richard Brimacombe[2] and Marin van Heel[1]*

Background: In recent years, the three-dimensional structure of the ribosome has been visualised in different functional states by single-particle cryo-electron microscopy (cryo-EM) at 13–25 Å resolution. Even more recently, X-ray crystallography has achieved resolution levels better than 10 Å for the ribosomal structures of thermophilic and halophilic organisms. We present here the 7.5 Å solution structure of the 50S large subunit of the *Escherichia coli* ribosome, as determined by cryo-EM and angular reconstitution.

Results: The reconstruction reveals a host of new details including the long α helix connecting the N- and C-terminal domains of the L9 protein, which is found wrapped like a collar around the base of the L1 stalk. A second L7/L12 dimer is now visible below the classical L7/L12 'stalk', thus revealing the position of the entire L8 complex. Extensive conformational changes occur in the 50S subunit upon 30S binding; for example, the L9 protein moves by some 50 Å. Various rRNA stem-loops are found to be involved in subunit binding: helix h38, located in the A-site finger; h69, on the rim of the peptidyl transferase centre cleft; and h34, in the principal interface protrusion.

Conclusions: Single-particle cryo-EM is rapidly evolving towards the resolution levels required for the direct atomic interpretation of the structure of the ribosome. Structural details such as the minor and major grooves in rRNA double helices and α helices of the ribosomal proteins can already be visualised directly in cryo-EM reconstructions of ribosomes frozen in different functional states.

Addresses: [1]Imperial College of Science Technology and Medicine, Department of Biochemistry, London SW7 2AY, UK and [2]Max-Planck-Institut für Molekulare Genetik, D-14195 Berlin, Germany.

*Corresponding author.
E-mail: m.vanheel@ic.ac.uk

Key words: angular reconstitution, cryo-electron microscopy, ribosomal proteins, ribosome structure, 50S ribosomal subunit

Received: 4 October 1999
Revisions requested: 15 October 1999
Revisions received: 4 November 1999
Accepted: 19 November 1999

Published: 2 December 1999

Structure December 1999, 7:1575–1583

0969-2126/99/$ – see front matter

Introduction

Ribosomes, the main players in messenger-directed protein synthesis, consist of a small and large subunit which meet upon initiation of protein synthesis. Ribosomes and ribosomal subunits can assume random orientations in vitreous ice preparations for cryo-electron microscopy (cryo-EM) [1,2] and these random orientations can be exploited for calculating full three-dimensional structures of these particles. The introduction of such zero-tilt techniques (e.g. the angular reconstitution approach [3]) to the study of the ribosome led to the first reproducible ribosomal structures at the 23–25 Å resolution level only a few years ago [2,4]. The *Escherichia coli* ribosome has since been studied in different functional states, such as the pre- and the post-translocational state [5], in which the aminoacyl-tRNA-binding site (A site) and peptidyl-tRNA-binding site (P site) tRNAs are directly visible. The various ribosome-associated factors, such as elongation factor Tu [6] and elongation factor G [7] (H stark, MV Rodnina, MVH and W Wintermeyer, unpublished results), can now be imaged *in situ* by blocking the ribosome with an appropriate antibiotic (e.g., kirromycin). Virtually all functional-state studies have hitherto been performed on the best characterised bacterial ribosome, the 70S *E. coli* ribosome.

For a long time it proved difficult to obtain good crystals of ribosomes or ribosomal subunits, and the progress with X-ray crystallography has accordingly been slow [8]. No crystals suitable for X-ray diffraction have been obtained of the *E. coli* ribosome or of its subunits. Good crystals have been obtained of the 50S ribosomal subunit from the halophilic archaebacterium *Haloarcula marismortui*, which diffract beyond ~3 Å resolution [8–10], and of the *Thermus thermophilus* 30S ribosomal subunit [10]. Very recently, the diffraction patterns of these crystals have been phased to resolution levels of 9 Å and 7 Å, respectively [9,10]; the initial crystallographic phase determination was, in part, aided by low-resolution cryo-EM reconstructions. The good quality of the X-ray crystals imply that high-resolution results may be anticipated in the near future.

Cryo-EM has an advantage over X-ray crystallography in that it does not require crystals and thus avoids long crystallisation procedures. Moreover, cryo-EM employs a

specimen preparation technique that takes only milliseconds (the actual freeze-plunging [1]), and is thus well suited for studying short-lived functional intermediate states of ribosomes from well-characterised organisms such as *E. coli*. A limiting factor for obtaining high-resolution results purely by cryo-EM is the precision with which the electron microscopical contrast transfer function (CTF) can be determined. The poor signal-to-noise ratios (SNR) inherent in low-dose electron images of vitreous-ice embedded specimens makes the precise determination of the CTF a difficult task (the poor SNRs in the images are a direct consequence of the low electron exposure levels that the radiation-sensitive biological samples can tolerate). As a consequence of this lack of precision, the high-resolution data components may be added to the data set with inconsistent phases, causing them to average out incoherently.

We have used here a novel CTF-correction algorithm, capable of finding subtle local defocus and astigmatism variations within a single micrograph, to determine the 7.5 Å cryo-EM structure of the *E. coli* 50S ribosomal subunit. To compare the results obtained for free 50S subunits with those in the complete 70S ribosome, we use a reconstruction of the kirromycin-stalled 70S complex [6], which was recently refined to ~13 Å resolution (H Stark, MV Rodnina, F Zemlin, W Wintermeyer and MVH unpublished results). We interpret our results using a preliminary 23S rRNA model [11,12], based upon the 13 Å reconstruction. Moreover, we found a study on the protection of 23S rRNA upon subunit binding [13] most helpful in the interpretation of our data.

Results and discussion

The 50S subunit samples were vitrified on holey carbon films and imaged in a Philips CM200 field emission gun (FEG) cryo-microscope at liquid nitrogen temperatures. The CTF correction was applied directly after digitisation of the micrographs; spatial frequencies of up to ~1/7.0 Å were successfully corrected. The final 50S three-dimensional reconstruction at 7.5 Å resolution represents one of the highest resolution structures derived from single-particle cryo-EM, and matches those obtained previously for highly symmetric icosahedral particles [14,15]. The resolution of this structure is similar to those achieved in recent X-ray diffraction studies of the *H. marismortui* 50S ribosomal subunit [9,10] and the *T. thermophilus* 30S subunit [10]. The isolated *E. coli* 50S ribosomal subunit is clearly a rigid and stable particle, amenable to high-resolution cryo-EM structural studies, as is the kirromycin-stalled 70S ribosome (H Stark, MV Rodnina, F Zemlin, W Wintermeyer and MVH, unpublished results). The map is of good quality in that it contains few densities unconnected to the main structure. Areas where a number of small unconnected densities do occur, such as the L1 protein area, seem to indicate some disorder due to local structural flexibility.

The 50S subunit at 7.5 Å resolution

The new high-resolution 50S subunit structure shows all of the classical features of this subunit, including the central protuberance (CP), the A-site finger (ASF), the L7/L12 stalk and the L1 protuberance (Figure 1). The improvement in linear resolution from the 15–18 Å level of earlier studies [6,16] to the current 7.5 Å, corresponds to an approximately tenfold increase in three-dimensional information content [17]. As a road map for interpreting our new high-resolution map, we made extensive use of the most recent version of the 23S rRNA model [11,12], which was fitted to the refined 13 Å map of the kirromycin-stalled 70S particles (H Stark, MV Rodnina, F Zemlin, W Wintermeyer and MVH, unpublished results). As this model (Figure 1c) had been fitted to the 30S-bound 50S subunit (Figure 1b), it also helped identification of the similarities and differences between the bound and free 50S structures. The new map also revealed 70S densities which, during the model building process, had been assigned to the wrong subunit. Following our philosophy of progressive improvements [11,12], the new cryo-EM map itself imposes new constraints on the 23S rRNA model and thus indicates where rearrangements of the model are required.

A large proportion of the free 50S structure is virtually indistinguishable from the bound 50S structure when viewed at the same resolution. In particular, the whole solvent-exposed side of the 50S subunit map shows no differences with respect to the bound 50S particle at 13 Å resolution (results not shown). In contrast to these extensive similarities, there are specific areas of the map where the densities are clearly different. In particular, some areas of the density around the peptidyl transferase centre (PTC) in the interface between the subunits are so different in both structures that it becomes difficult to localise corresponding structural details. We refer to the cleft in which the PTC is localised as the 'PTC cleft'. In the following, we mainly concentrate on the areas of the 50S structure that are involved in binding the 30S subunit, most of which show clear — sometimes dramatic — conformational changes with respect to the bound state of the 50S subunit.

The L9 protein

A prominent new structural detail in the isolated 50S subunit is the L1 stalk collar, which wraps around the lower part of the L1 stalk (Figures 1–3). The collar is on one side of the stalk and is attached to its base. The collar includes a long, fully solvent-exposed rod-like structure located between two apparently rRNA-bound globular domains. This shape corresponds well with that of the structure of the L9 ribosomal protein determined by the combined use of X-ray crystallography and nuclear magnetic resonance (NMR) spectroscopy [18]. The L9 structure comprises two separate rRNA-binding domains

Figure 1

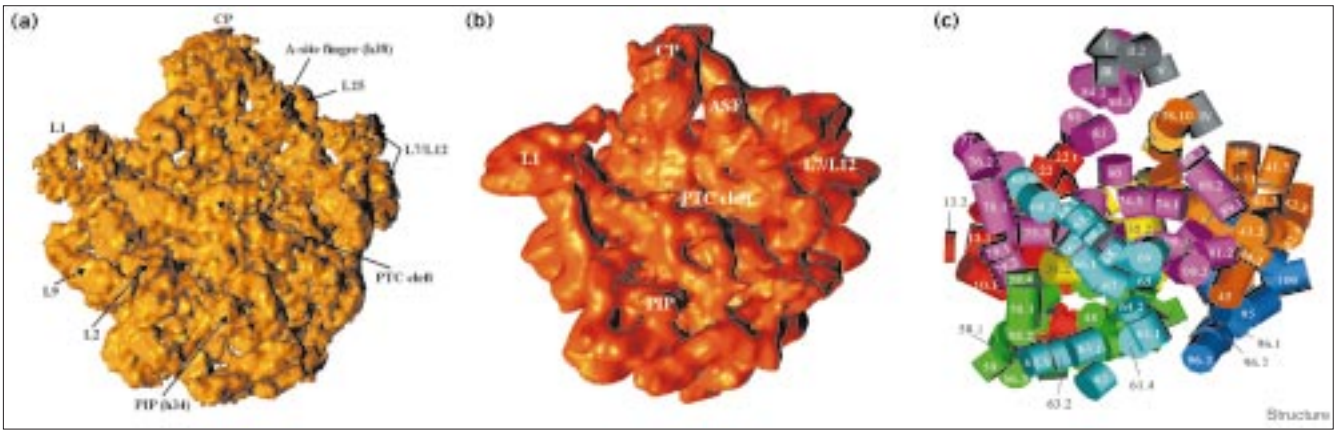

Surface representations of the *E. coli* 50S ribosomal subunit viewed from the subunit interface side. (a) The 50S subunit in its classical 'crown' view. Classical features are indicated: the L1 protuberance, the central protuberance (CP), and the L7/L12 protuberance. The A-site finger (ASF), located between CP and the L7/L12 region, is the position of h38 (part of the 890 hairpin loop) which cross-links to the elbow region of the A-site tRNA. The protrusion which extends to within the boundaries of the 30S subunit in the 70S complex (the PIP) is believed to contain helix h34 (part of the 715 hairpin loop). The peptidyl transferase centre lies within the cleft marked 'PTC cleft'. Preliminary fits of the structure of an L2 protein fragment and an L25–rRNA complex are indicated, as is the position of the L9 protein. A considerable rearrangement of the PTC cleft densities occurs upon 30S binding. (b) The 50S subunit separated interactively from a 13 Å resolution reconstruction of the full 70S ribosome stalled by the antibiotic kirromycin, which prevents dissociation of the elongation factor Tu from the ribosome (H Stark, MV Rodnina, F Zemlin, W Wintermeyer and MVH, unpublished results). The differences in appearance between this 50S subunit and the free 50S subunit (a) are discussed in the text. (c) Helical regions of the 23S rRNA, modelled into the 13 Å *E. coli* 70S ribosome cryo-EM map. The model is in the same orientation as parts (a) and (b) and various relevant sites are marked. The ASF is close to helix II and III of the 5S rRNA in the central protuberance region of the free 50S particle. Helix h69 (part of the 1920 hairpin loop) on the ridge of the PTC cleft, moves towards the 30S subunit upon subunit association and is then in close contact to the decoding centre in the small subunit. Major conformational changes occur in this area of the structure upon subunit binding, which probably leads to the formation of the interface bridge.

connected by a long, rigid, and hydrophilic α helix, and we have successfully docked this model into the collar structure (Figure 3a). Protein L9 had previously been localised under the L1 protuberance by immunoelectron microscopy [19] and cross-linking experiments.

As seen in Figure 3a, the C-terminal domain and α helix fit unambiguously into the collar region density. The resolution in the 7.5 Å map is sufficient to allow the localisation of the small α helix (residues Ser95–His106 in *Bacillus stearothermophilus*) of the C-terminal domain, as well as the β turn His134–Val137, and loop features between residues Leu117–Ile121 and Ala83–Gly87. These and other details of both the N- and C-terminal domains of the L9 structure unambiguously define its orientation in the 50S subunit. Furthermore, the proposed rRNA-binding residues, Phe90 and Arg122 (Figure 3a), are in direct contact with the L1 stalk. We find that the N-terminal domain must undergo some interdomain rearrangement, however, in order to occupy the density at the other end of the α helix. In the 50S subunit, L9 appears more compact with the N-terminal domain twisted inwards towards the α helix and contacting rRNA. The long α helix (residues Pro41–Lys74 in *B. stearothermophilus*) is exceptionally stable [20] and, although the residues in this helix are not conserved, the length of the helix is preserved [18]. The structure of the N-terminal domain of L9 was poorly defined by X-ray data alone and the current model was refined in combination with NMR data [18], although high temperature factors in the N-terminal domain persist. All this suggests that the region has a conformational flexibility, and that a hinge region between the domain and the long α helix and/or within the long α helix is certainly possible. Such hinge regions could facilitate the docking of the N-terminal domain (a structural homologue of the crystallised C-terminal L7/L12 fragment [18]) to its rRNA substrate.

Most intriguingly, this new L9 structural detail is completely missing from the corresponding location in all previous reconstructions of the *E. coli* 70S ribosome [5,6,16], including the latest 13 Å reconstruction of the kirromycin-stalled 70S ribosome. Although most earlier reconstructions had been performed at lower resolution, in isolated 50S subunits this collar was clearly identifiable in three-dimensional reconstructions at ~15 Å resolution. Thus, the L9 protein appears to be missing at this position within the 70S complex (Figure 3b). The 50S complexes studied were derived from purified 70S ribosomes. Thus, L9 is unlikely to be present in the 50S if it were genuinely

Figure 2

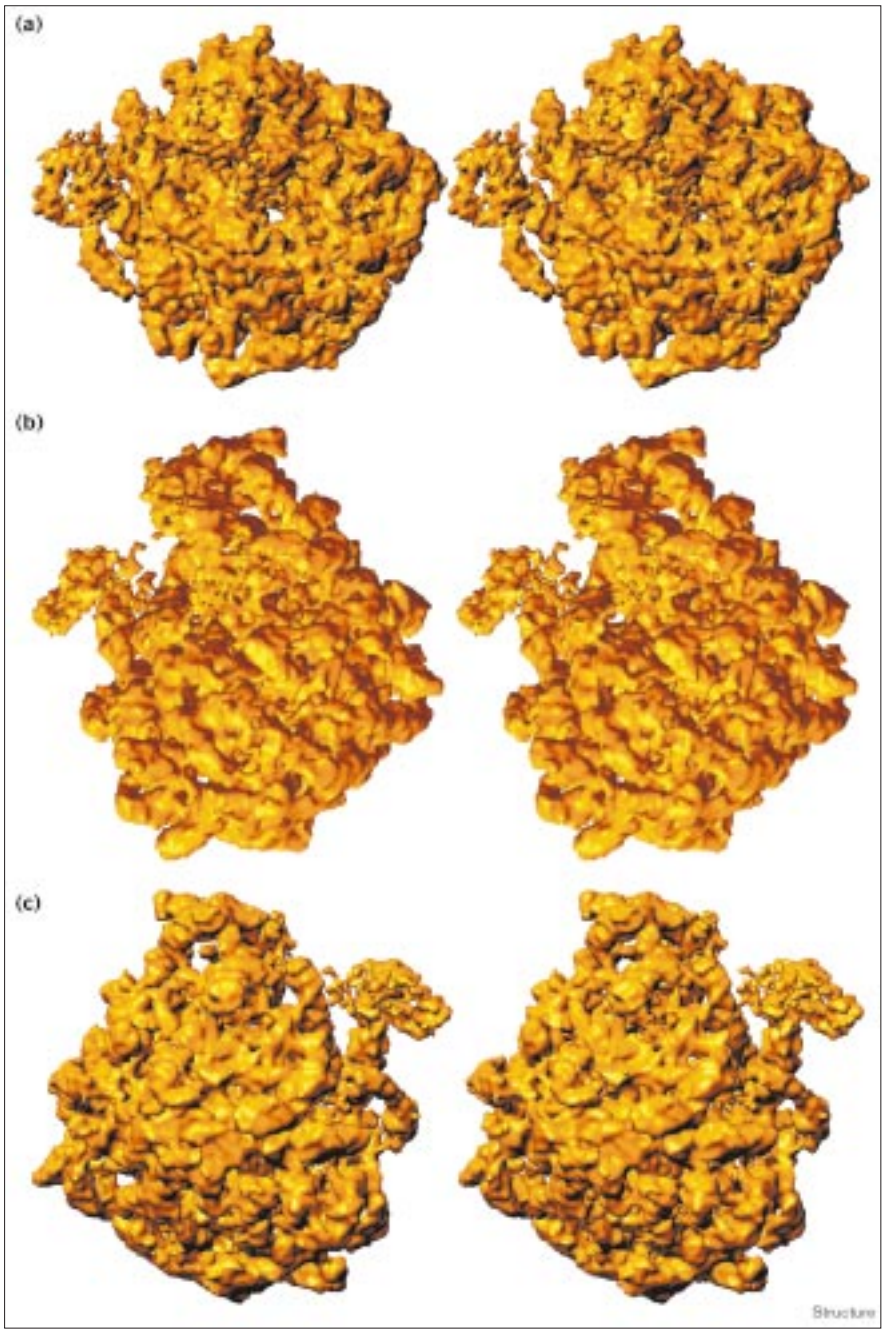

Stereoviews of the free *E. coli* 50S ribosomal subunit. (a) View from the subunit interface side along the direction of the exit channel. Around the entrance of the exit channel/tunnel is the location of the peptidyl transferase centre (PTC). (Comparable viewing directions were used for illustrations in [9] and [25].) (b) The 50S subunit from the L7/L12 side. This orientation gives a view along the full-length PTC cleft. (c) The L1 side of the 50S subunit. The mushroom-shaped L1 protuberance is clearly visible on the right-hand side of the illustration. Wrapped around the stalk is the L9 protein. The long hydrophilic α helix connecting the N- and C-terminal domains of L9 is seen here to be fully solvent-exposed.

missing from the 70S complex. The exact position of L9 within the 70S ribosome thus presents an intriguing question. A careful study of the 13 Å 70S map reveals a strut-like structure (Figure 3b), which is part of the 50S–30S interface and appears to end in the top of the L1 protuberance. This structure could hold the full L9 protein; it is the candidate structure that is physically closest to the position of the L9 protein in free 50S. The two positions are separated by a distance of some 50 Å.

The A-site finger

A conformational change takes place in the A-site finger (ASF) region [5]. In the 70S ribosome the ASF connects to the head of the 30S subunit [5], whereas in the isolated 50S subunit the ASF bridges to the central protuberance (CP; Figure 1a). The elbow region of the A-site-bound tRNA has been cross-linked to h38 of the 23S rRNA [21]. The 890 stem-loop region was also implicated in intersubunit contacts from protection studies [13]. Of the 5S RNA

Figure 3

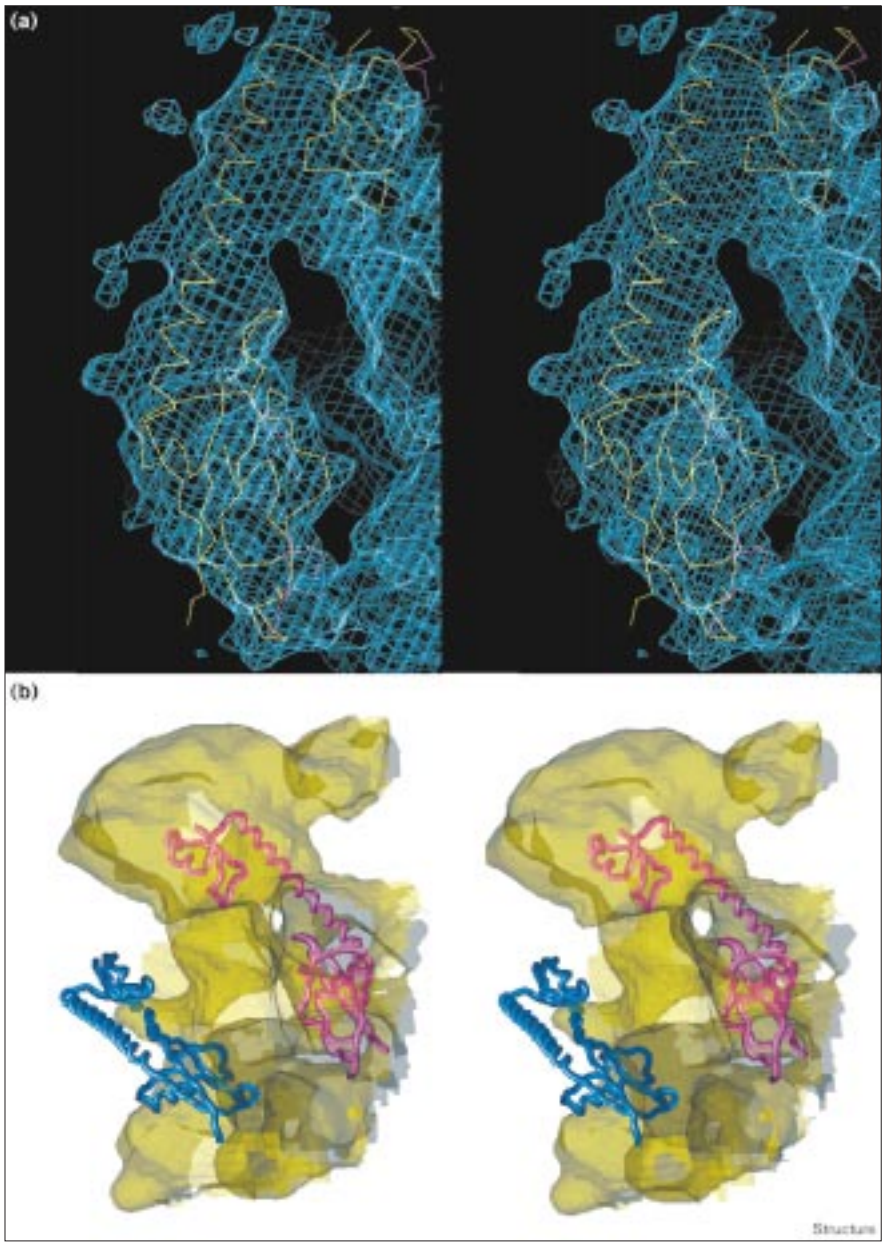

Fitting of the *B. stearothermophilus* L9 protein (PDB accession code 1DIV) into the three-dimensional density of the collar structure around the L1 stalk of the 7.5 Å *E. coli* 50S ribosomal subunit. The coordinates were fitted interactively into the cryo-EM density using the program O [39]. To emphasise the quality of the fit to the level of fine detail, the cryo-EM map was high-pass filtered more strongly than the other maps in this study. The shape of the N-terminal domain (upper domain) is directly recognisable in the cryo-EM map, but its relative position with respect to the C-terminal domain differs from that in the crystal. (b) View of the corresponding area in the 13 Å three-dimensional reconstruction of the kirromycin-stalled 70S ribosome. The position of the L9 protein in the free 50S subunit is shown in blue. Even though the threshold value used here for rendering the reconstruction was lower than the corresponding density used for rendering the free 50S reconstruction, no density is seen in this area of the map. Within the 30S–50S interface area, a possible location of the L9 protein is indicated by the second cartoon representation of the L9 protein (pink).

helices (nomenclature as in [11]), the HII and HIII cross-link to the 890 region of h38 [22]. Thus we have modelled (Figure 1c) the 890 region of the 23S rRNA into the ASF structure [11,12].

The principal interface protrusion

The face of the isolated 50S subunit that meets the 30S subunit in the 70S ribosome is remarkably flat. The one protrusion that trespasses this flat surface we call the 'primary interface protrusion' (PIP); it is located below the PTC cleft at about one third of the full height of the subunit (Figures 1a,2a,b,4a). This PIP structure could already be clearly discerned in early reconstructions of the 70S ribosome [2,4], but in those early studies the PIP was marked only as one of a number of intersubunit connections and its prominent character in free 50S particles had not been recognised. The protrusion had not been assigned any rRNA structure in our most recent 23S rRNA model [11,12], as we originally thought the PIP to be associated with the L2 protein. In our current 7.5 Å map, however, this structural detail has unequivocally taken the characteristic shape of an rRNA hairpin loop. Thus, we now believe that PIP probably represents the h34 helix which was placed somewhat further back in our 23S rRNA

Figure 4

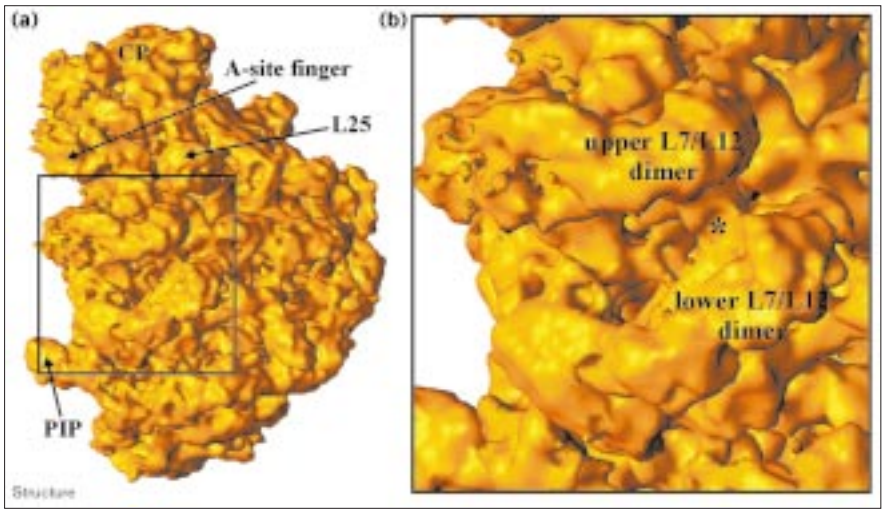

Side view of the *E. coli* 50S ribosomal subunit from the L7/L12 side. This view indicates how the L8 complex is placed in the large subunit (see text for details). The PIP is the main protrusion in the interface area of the large ribosomal subunit. **(b)** Magnified view of the L8 area containing two L7/L12 dimers and the L10 protein. The 'upper' L7/L12 dimer had been identified in previous cryo-EM reconstructions. A potential 'lower' L7/L12 dimer has now been identified in the new reconstruction. The density connecting the two dimers, indicated by a star, may correspond to the L10 protein.

model. This helix has been implicated in binding to the small subunit in a recent chemical protection study [13]. In the 70S complex, the PIP structure remains virtually unchanged and penetrates deep into the 30S subunit in the central domain area of 16S rRNA, where the footprints of ribosomal proteins S6 and S18 are located [23,24].

The PTC cleft

The PTC cleft is a long 'canyon' along the surface of the 50S subunit through which the CCA ends of the tRNA pass during the elongation cycle [5]. An interesting conformational change in the 50S subunit, which occurs upon the binding of the 30S subunit, is the opening of the PTC cleft. This widening of the PTC cleft apparently facilitates access to the PTC area around the entrance of the exit channel. We have assigned the density on the top edge of the PTC cleft to h69 of the 23S rRNA [11,12]. In the 70S structure, this helix is in direct interaction with the decoding centre on the 30S subunit [11,12]. In the protection experiments of Merryman *et al.* [13], the kethoxal reactivity of G2505 in the central loop of the 23S rRNA domain V — known to be strongly associated with peptidyl transferase activity — was found to increase sharply upon 30S binding. The increased chemical accessibility of the PTC supports the structural opening we find. The PTC cleft is a structurally conserved element in all species [9,25]; apparently also evolutionarily conserved is the PTC cleft opening upon subunit binding. It can be clearly seen that the large subunit within the 80S mammalian ribosomal complex [25] is in the open conformation, whereas the individual 50S subunit of *H. marismortui* [9] is in the closed conformation.

The L7/L12 'stalk' region

An intriguing observation can be made in the L7/L12 area of the 50S subunit. The extended stalk conformation, which is well known from traditional negatively stained specimens prepared on carbon foils, is not normally found in cryo-EM preparations. Rather than protruding from the 50S contour, in cryo-EM preparations the L7/L12 stalk is found to be bent inwards, following the outer contour of the 50S particle [4,5]. Extended stalks have been observed in cryo-EM preparations, but normally only in specimens prepared on charged carbon support films [16]. Careful examination of the whole L7/L12 area in our new three-dimensional reconstruction reveals some interesting details. Below the L7/L12 stalk — and largely parallel to this structure — a second stalk-like structure has become visible (Figures 2a,b,4).

At lower resolution, the second stalk-like density is not clearly distinguishable from a density rod immediately behind it and together they appear to represent a single entity. At the current increased resolution, however, the lower stalk has assumed its own structural identity and in its details starts to resemble the 'original' L7/L12 stalk directly above it. It is known that two L7/L12 dimers (the 24 kDa dimer consisting of the two identical 12 kDa L7 and L12 monomers) bind to the ribosome [26]. Thus, we have here potential candidate density for the second L7/L12 dimer (Figure 4b), and hence — by implication — the entire 'L8' assembly comprising two copies of the L7/L12 dimer and the L10 protein to which the N-terminal domains of all four L7/L12 chains bind. These results appear compatible with previous data [26,27]. The density connecting the two dimers is a plausible candidate for the L10 protein.

The L8 complex (L10–$(L7/L12)_4$) is essential for the functioning of the ribosome and the whole L8 complex may be exchanged between 50S subunits of different species, thus creating functioning chimeric ribosomal subunits [28].

Figure 5

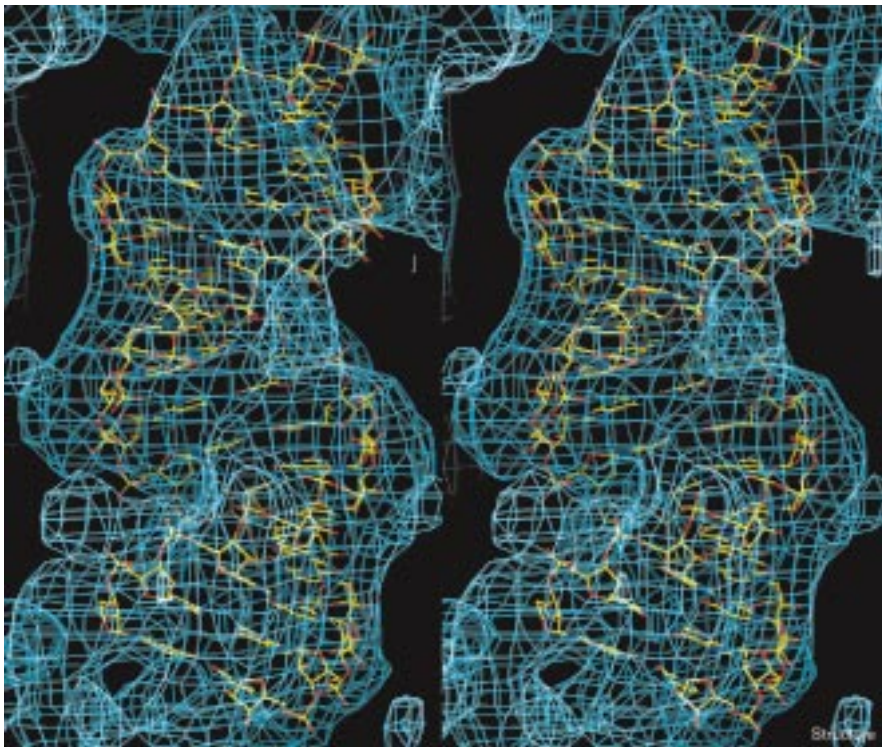

Fitting of an rRNA helical region of unknown sequence into the 7.5 Å resolution map of the *E. coli* 50S ribosomal subunit. At this resolution level the major and minor grooves of the duplex can clearly be recognised. The coordinates of a generic RNA helix were located during a real-space template search using the program ESSENS [38].

Comparison with the 50S subunit of *H. marismortui*

Our 7.5 Å reconstruction of the *E. coli* subunit clearly resembles the recent 9 Å X-ray structure of the *H. marismortui* large ribosomal subunit [9]. For example, the long ridge of rRNA helices, demarcating the top edge of the PTC cleft towards the L1 protuberance side of the subunit, looks virtually identical in both maps. The similarity extends to even the minute details of the shallow minor grooves of the double-stranded rRNA helices in this area. The quality of the cryo-EM map in elucidating such details is highlighted in Figure 5. At the same time, there are areas of the maps that reflect unambiguous structural differences between these species. For example, the L9 protein discussed above is missing from the *H. marismortui* map while the L1 stalks are almost indistinguishable. Major structural differences are also observed in the region where we believe protein L25 to be located (Figure 1), on the basis of a preliminary fit of the atomic coordinates of an L25–rRNA complex (M Stoldt, J Wöhnert, O Ohlenschäger, M Görlach and LR Brown, personal communication); again, the *E. coli* protein L25 has no equivalent in *H. marismortui*.

Discussion of recently published X-ray structures

Following the first submission of this manuscript, a number of papers appeared describing the X-ray structures of ribosomes and ribosomal subunits [29–32]. These X-ray structures (and our cryo-EM structure) were presented at the International Ribosome meeting in Helsingør, Denmark, in June 1999, and these results are now reaching print. Although the various structures resemble each other in most (conserved) details, the interpretations of the maps at this — for X-ray crystallography — intermediate level of resolution are not entirely in agreement. For example, an L11–rRNA complex has been interpreted in an area which in all earlier cryo-EM structures and the X-ray structure [32] of the 70S *T. thermophilus* ribosome was interpreted as the (upper) L7/L12 dimer. It is obvious that the interpretations will converge to a consensus structure, as the various techniques yield structures at increasing resolution levels.

In order to better compare the results obtained using different approaches, it is necessary to have a more liberal exchange of the experimental data. Similar to the traditions existing in high-resolution X-ray crystallography where the atomic coordinates must often be made available within a year of publication, medium-resolution three-dimensional density maps determined by cryo-EM or X-ray crystallography should also become generally accessible. Our new 7.5 Å structure will be freely available within one year after publication of this paper.

Biological implications

The 7.5 Å resolution three-dimensional structure of the isolated 50S ribosomal subunit from *Escherichia coli* illustrates the power of the angular reconstitution cryo-EM

approach in visualising the functioning ribosome. Complementary structures can be obtained without the need to grow three-dimensional crystals, and without the constraints imposed by crystal contacts. It is clear from our structural studies of both the large ribosomal subunit and the full ribosome, that the 70S ribosome is more than just the sum of its two main components. The intricate intermingling of the 30S and 50S components at the interface of the large and small ribosomal subunits make it difficult to assign density elements specifically to one of the two subunits. This type of problem is exemplified by the behaviour of the ribosomal protein L9, which appears to have moved from its position in free 50S to the 30S–50S interface area within the 70S complex. In this interface area, L9 appears to be enveloped in structural elements arising from the small subunit. In light of the large conformational changes found, interpretation of the earlier biochemical data in terms of proximities of the ribosomal components may be difficult without a detailed knowledge of the exact state of the ribosome or its components. It may be expected, however, that the ambiguities in the subunit interface region will be resolved when further high-resolution cryo-EM structures of different relevant ribosomal complexes become available.

We are in the process of refining our 23S rRNA model [11,12] to incorporate the new 7.5 Å information. Now we can directly identify even relatively small α helices of the ribosomal proteins, the quality of the rRNA and protein-fitting maps will improve considerably. Whereas in the earlier version of the model the (more indirect) biochemical information played a primary role, the directly recognisable structural elements in the new 7.5 Å map are becoming increasingly important anchor points for building our next-generation models. In order to fully understand the conformational changes taking place within the 50S subunit upon binding of the 30S ribosomal subunit, we will eventually need atomic-resolution structures of both the isolated large ribosomal subunit and the full 70S complex. Although further technological developments are required to reach quasi-atomic resolution levels by cryo-EM (better than ~4 Å), there are no fundamental limitations in sight to prevent us from reaching that goal. In the process, we are obtaining better and better three-dimensional insight into a most fascinating and complex molecular machine.

Materials and methods

Salt-washed *E. coli* 50S ribosomal subunits (MRE-600) were purified by zonal centrifugation using standard procedures, applied to a holey carbon film, and freeze-plunged into liquid ethane after blotting off excess fluid. The vitrified 50S sample was subsequently imaged in a Philips CM200 FEG electron cryo-microscope at liquid-nitrogen temperatures, using a Gatan side-entry cryo-holder and cryo-transfer system. The images were taken at defocus values ranging from 10,000–20,000 Å underfocus, at an electron-optical magnification of 38,000.

Good micrographs (verified by optical diffraction) were digitised using the Image Science patchwork densitometer (M Schatz *et al.*, unpublished results) using a step size of 5μm × 5μm, corresponding to 1.32 Å × 1.32 Å on the specimen scale leading to 256 × 256 pixel 50S subunit images. For the final analysis, this sampling distance, leading to 256 × 256 pixel 50S subunit images, was re-interpolated to an effective sampling of 1.76 Å × 1.76 Å by masking of the Fourier transforms of the raw images down to 192 × 192 pixels. The densitometry and all subsequent image processing were performed within the IMAGIC-5 software system [33] under the Linux, DEC-Unix, Compaq Tru64 UNIX and Windows-98 operating systems. After digitisation of the micrographs, the CTF was corrected using a newly developed program implemented in the context of the IMAGIC-5 software package. This program matches the modulus of the theoretical two-dimensional CTF – including astigmatism – with the local two-dimensional amplitude spectrum of the electron micrographs by cross-correlation (AP *et al.*, unpublished results). The program allows the user to make several CTF measurements over a micrograph using typically ~2048 × 2048 pixel patches. Local defocus parameters – specific for the position of each particle image individually – are then estimated by linear interpolation of the defocus values found for the positions of the various 2048 × 2048 patches; thus, accounting for unintended tilts of the specimen holder and non-flat fields of view. Based on the estimated local defocus parameters, the phases beyond each CTF zero crossing were simply reversed, without affecting the corresponding amplitudes. We were successful in correcting the CTF to the sixth to eighth zero crossing, which at the defocus values of 1.0–2.0 μm used in the study corresponds to spatial frequencies of ~1/7 Å.

All subsequent data analysis procedures were similar to the angular reconstitution [3] procedures used in previous studies [5,6,17]. The full data set comprised ~16,000 particles selected from seven micrographs. We used a 50S subunit extracted interactively from an earlier 70S *E. coli* three-dimensional reconstruction [6] as a starting point for our refinement procedure. A large set of reprojections of this model was used for multireference alignment of the first part of the data set (the large defocus images, 2.0 μm) of the isolated 50S particles. The iterative angular reconstitution procedures rapidly converged towards the properties of the free 50S data set alone. Our procedures comprised of multireference alignments (MRA), multivariate statistical data compression and automatic classification [34], angular reconstitution Euler angle assignments [3] with respect to an anchor set of projections [33], three-dimensional reconstruction [35], and creating new MRA references by reprojection for further iterations of the three-dimensional analysis [33]. The eigenvectors of the data set did not indicate any significant magnification variations within the data set [36], from which we concluded that the magnification variations were smaller than ~0.5% and did not require explicit correction [37]. The final resolution in the reconstruction was assessed by Fourier shell correlation [35] using the 3σ threshold criterion [17]. For the final representation of the results, the low-frequency components of the three-dimensional map were suppressed by a Gaussian high-pass filter with a 1/e width corresponding to ~1/25 Å. The multiplicative Fourier-space filter is $\{1 - \exp(-f^2 / \sigma^2)\}$; whereby f represents the distance to the origin of the three-dimensional Fourier volume, and σ is the 1/e width of the filter. For localising ribosomal protein and rRNA structures into our map we used an array of different programs. The L25–rRNA complex was found automatically using the ESSENS [38] real-space correlation program; the L9 protein was fitted into the density using both 'O' [39] and ERNA3D [23]; the rRNA fits were also performed with both these programs. The 23S rRNA models fitted by ERNA3D have now also been energy minimised (I Sommer and RB, unpublished results).

Acknowledgements

We thank Michael Schatz and Ralf Schmidt of Image Science, Berlin for help with the IMAGIC software system, Robert Finn for sequence analysis of the L9 protein, Holger Stark for his contributions during the early phases of the processing and Melanie Morris for editorial assistance. Matthias Görlach made the coordinates of the L25 protein–rRNA complex available

prior to publication. Our work was financed in part by European Commission grants. The farm of Compaq EV6 computers used for alignment refinements was financed by the BBSRC Centre of Structural Biology grant. The CM-200/FEG microscope was funded by BBSRC/HEFCE Joint Research Equipment Initiative grant.

References

1. Dubochet, J., *et al.*, & Schultz, P. (1988). Cryo-electron microscopy of vitrified specimens. *Quart. Rev. Biophys*. 21, 129-228.
2. Stark, H., *et al*., & Van Heel, M. (1995). The 70S *Escherichia coli* ribosome at 23 Å resolution: fitting the ribosomal RNA. *Structure* 3, 815-821.
3. Van Heel, M. (1987). Angular reconstitution: *a posteriori* assignment of projection directions for 3D reconstruction. *Ultramicroscopy* 21, 111-124.
4. Frank, J., *et al.*, & Agrawal, R.K. (1995). A model of protein synthesis based on cryo-electron microscopy of the *E. coli* ribosome. *Nature* 376, 441-444.
5. Stark, H., *et al.*, & Van Heel, M. (1997). Arrangement of the tRNAs in pre- and post-translocational ribosomes revealed by electron cryomicroscopy. *Cell* 88, 19-28.
6. Stark, H., Rodnina, M.V., Rinke-Appel, J., Brimacombe, R., Wintermeyer, W. & Van Heel, M. (1997). Visualisation of elongation factor Tu on the *Escherichia coli* ribosome. *Nature* 389, 403-406.
7. Agrawal, K.R., Penczek, P., Grassucci, R.A. & Frank, J. (1998). Visualization of the elongation factor G on *E. coli* 70S ribosome: the mechanism of translation. *Proc. Natl Acad. Sci.* 95, 6134-6138.
8. Yonath, A. & Berkovitch-Yellin, Z. (1993). Hollows, voids, gaps and tunnels in the ribosome. *Curr. Opin. Struct. Biol*. 3, 175-181.
9. Ban, N., *et al*., & Steitz, T.A. (1998). A 9 Å resolution X-ray crystallographic map of the large ribosomal subunit. *Cell* 93, 1105-1115.
10. Harms, J., *et al.,* & Yonath, A. (1999). Elucidating the structure of ribosomal particles: an interplay between electron-cryo-microscopy and X-ray crystallography. *Structure* 7, 931-941.
11. Brimacombe, R., Greuer, B., Mueller, F., Osswald, M., Rinke-Appel, J., & Sommer, I. (1999). Three-dimensional organisation of the bacterial ribosome and its subunits: the transition from low-resolution models to high-resolution structures. In *The Ribosome; Structure, Function, Antibiotics, and Cellular Interactions*. (Garrett, R.A., Douthwaite, S.R., Liljas, A., Matheson, A.T., Moore, P.B. & Noller, F.F., eds), ASM Press, Washington DC, in press.
12. Brimacombe, R. (1999). The structure of ribosomal RNA. *ASM Newsletter* 6, 144-151.
13. Merryman, C., Moazed, D., Daubresse, G. & Noller, H.F. (1999). Nucleotides in 23S rRNA protected by the association of 30S and 50S ribosomal subunits. *J. Mol. Biol.* 285, 107-113.
14. Conway, J., Cheng, N., Wingfield, P.T., Stahl, S.J. & Steven, A.C. (1997). Visualisation of a 4-helix bundle in the hepatitis B virus capsid by cryo-electron microscopy. *Nature* 385, 91-94.
15. Böttcher, B., Wynne, S.A. & Crowther, R.A. (1997). Determination of the fold of the core protein of hepatitis B virus by electron cryomicroscopy. *Nature* 386, 88-91.
16. Malhotra, A., *et al*., & Frank, J. (1998). *E. coli* 70S ribosome at 15 Å resolution by cryo-electron microscopy: localization of fMet–tRNA^{fMet} and fitting of L1 protein. *J. Mol. Biol.* 280, 103-115.
17. Orlova, E.V., *et al*., & Van Heel, M. (1997). Structure of keyhole limpet hemocyanin type 1 (KLH1) at 15 Å resolution by electron cryomicroscopy and angular reconstitution, *J. Mol. Biol*. 271, 417-437.
18. Hoffman, D.W., Cameron, C.S., Davies, C., White, S. & Ramakrishnan, V. (1996). Ribosomal protein L9: a structure determination by the combined use of X-ray crystallography and NMR spectroscopy. *J. Mol. Biol*. 264, 1058-1071.
19. Stöffler-Meilicke, M., Noah, M., & Stöffler, G. (1983). Location of eight ribosomal proteins on the surface of the 50S subunit from *Escherichia coli*. *Proc. Natl Acad. Sci. USA* 80, 6780-6784.
20. Kuhlman, B., Yang, H.Y., Boice, J.A., Fairman, R. & Raleigh, D.P. (1997). An exceptionally stable helix from the ribosomal protein L9: implications for protein folding and stability. *J. Mol. Biol.* 270, 640-647.
21. Rinke-Appel, J., Jünke, N., Osswald, M. & Brimacombe, R. (1995). The ribosomal environment of tRNA:cross-links to rRNA from positions 8 and 20:1 in the central fold of tRNA located at the A, P or E site. *RNA* 1, 1018-1028.
22. Osswald, M. & Brimacombe, R. (1999). The environment of 5S rRNA in the ribosome: cross-links to 23S rRNA from sites within helices II and III of the 5S molecule. *Nucleic Acids Res*. 27, 2283-2290.
23. Mueller, F. & Brimacombe, R. (1997). A new model for the three-dimensional folding of *Escherichia coli* 16S ribosomal RNA. I. Fitting the RNA to a 3D electron microscopic map at 20 Å. *J. Mol. Biol.* 271, 524-544.
24. Mueller, F. & Brimacombe, R. (1997). A new model for the three-dimensional folding of *Escherichia coli* 16S ribosomal RNA. II. The RNA–protein interaction data. *J. Mol. Biol.* 271, 545-565.
25. Dube, P., *et al*., & Van Heel, M. (1998). The 80S rat liver ribosome at 25 Å resolution by electron microscopy and angular reconstruction. *Structure* 6, 398-399.
26. Traut, R.R., *et al*., & Jameson, D. (1995). Location and domain structure of *Escherichia coli* ribosomal protein L7/L12: site specific cysteine crosslinking and attachment of fluorescent probes. *Biochem. Cell Biol.* 73, 949-958.
27. Möller, W. & Maassen, J.A. (1986). On the structure, function, and dynamics of L7/L12 from *Escherichia coli* ribosomes. In *Structure, Function, and Genetics of Ribosomes.* (Hardesty, B. & Kramer, G., eds), Springer-Verlag, Berlin.
28. Stöffler-Meilicke, M. & Stöffler, G. (1991). The binding site of ribosomal protein L10 in eubacteria and archaebacteria is conserved: reconstitution of chimeric 50S subunits. *Biochimie* 73, 797-804.
29. Ban, N., Nissen, P., Hansen, J., Capel, M., Moore, P.B. & Steitz, T.A. (1999). Placement of protein and RNA structures into a 5 Å resolution map of the 50S ribosomal subunit. *Nature* 400, 841-847.
30. Clemons, W.M. Jr, May, J.L., Wimberly, B.T., McCutcheon, J.P., Capel, M.S. & Ramakrishnan, V. (1999). Structure of a bacterial 30S ribosomal subunit at 5.5 Å resolution. *Nature* 400, 833-840.
31. Culver, G.M., Cate, J.H., Yusupova, G.Z., Yusupov, M.M. & Noller, H.F. (1999). Identification of an RNA–protein bridge spanning the ribosomal subunit interface. *Science* 285, 2133-2136.
32. Cate, J.H., Yusupov, M.M., Yusupova, G.Z., Earnest, T.N. & Noller, H.F. (1999). X-ray crystal structures of 70S ribosome functional complexes. *Science* 285, 2095-2104.
33. Van Heel, M., Harauz, G., Orlova, E., Schmidt, R. & Schatz, M. (1996). A new generation of the IMAGIC image processing system. *J. Struct. Biol.* 116, 17-24.
34. Van Heel, M. (1989). Classification of very large electron microscopical image data sets. *Optik* 82, 114-126.
35. Harauz, G. & Van Heel, M. (1986). Exact filters for general geometry three-dimensional reconstruction. *Optik* 73, 146-156.
36. Bijlholt, M.M.C., Van Heel, M.G. & Van Bruggen, E.F.J. (1982). Comparison of 4×6-meric hemocyanins from three different arthropods using computer alignment and correspondence analysis. *J. Mol. Biol.* 161, 139-153.
37. Aldroubi, A., Trus, B.L., Unser, M., Booy, F.P. & Steven, A.C. (1992). Magnification mismatches between micrographs: corrective procedures and implications for structural analysis. *Ultramicroscopy* 46, 175-188.
38. Kleywegt, G.J. & Jones, T.A. (1997). Template convolution to enhance or detect structural features in macromolecualr electron-density maps. *Acta Crystallogr. D* 53, 179-185.
39. Jones, T.A. & Kjeldgaard, M. (1997). Electron-density map interpretation. *Methods Enzymol.* 277 *B*, 173-207.